ELSEVIER

Journal of Molecular Catalysis A: Chemical 111 (1996) 341–356

JOURNAL OF MOLECULAR CATALYSIS A: CHEMICAL

Structure of catalytic active site for oxidation of methane to methanol by H_2–O_2 gas mixture over iron-containing catalysts

Ye Wang, Kiyoshi Otsuka *

Department of Chemical Engineering, Tokyo Institute of Technology, Ookayama, Meguro-ku, Tokyo 152, Japan

Received 29 February 1996; accepted 29 April 1996

Abstract

Three model catalysts were designed to study the structure of the active iron site responsible for the conversion of methane to methanol by oxygen in the presence of hydrogen at atmospheric pressure. The catalytic activities were correlated with the characterizations of the coordination environments of the iron sites in the three model catalysts. The results suggest that the tetrahedrally coordinated iron site isolated from each other by phosphate groups is the active site for the selective oxidation of methane to methanol by H_2–O_2 gas mixture. The same iron site was effective for the conversion of methane to methanol by H_2O_2 or N_2O. The comparison studies among $FePO_4$, $FeAsO_4$ and $FeSbO_4$ indicate that the acidity of the surrounding groups of iron site plays important roles in the oxidation of methane with H_2–O_2 gas mixture. It is proposed that H_2 and O_2 are activated on the active iron site through the redox between Fe(III) and Fe(II), producing an adsorbed peroxide species responsible for the selective oxidation of methane to methanol. The isolated structure of iron sites must increase the steady-state concentration of the peroxide species generated from the reaction of H_2 and O_2 on the catalyst surface. The acidic groups surrounding the iron site serve as the acceptor and donor of protons and thus enhance the formation of the peroxide. Furthermore, the acidity of the surrounding groups of iron is suggested to contribute to the selective formation of CH_3OH through the protonation of the intermediate methoxide.

Keywords: Active site; Methane; Methanol; Iron-containing solid catalysts

1. Introduction

Direct oxidation of methane to methanol is one of the most challenging subjects in catalysis. It is well known that methane monooxygenase (MMO) in methanotrophic bacteria catalyzes the selective oxidation of methane to methanol by oxygen under ambient conditions [1,2]. However, such selective oxidation remains unsuccessful if we use synthetic catalysts. Particularly, it is extremely difficult to produce methanol from direct oxidation of methane by using solid catalysts [3–5]. The iron centers of MMO and cytochrome P-450 monooxygenase (heme iron and μ-oxo-bridged binuclear iron center, respectively) play the vital role as the

* Corresponding author. Tel.: +81-3-57342144; fax: +81-3-57342144; e-mail: kotsuka@o.cc.titech.ac.jp.

PII S1381-1169(96)00177-X

catalytic active sites in the monooxygenation of various substrates. Therefore, we believe that an iron-containing solid catalyst could be a promising one for the selective oxidation of methane to methanol if the iron site is situated in proper structural conditions.

So far, there are several reports showing that some iron-containing catalysts are active for the partial oxidation of methane. Lyons and coworkers [6] have shown that an [Fe]SOD catalyst (> 10 wt% Fe in sodalite zeolite) catalyzes oxidation of methane to methanol at > 400°C and at a pressure of 800 psi g (54.4 atm). Although a high selectivity to CH_3OH has been obtained in this case, the homogeneous radical reactions in the gas phase prevail at such a high reaction pressure, and thus it is difficult to evaluate the role of catalyst. In fact, it has been confirmed that the empty reactor tube is more effective for methanol production than the one containing an [Fe]SOD catalyst under such reaction conditions [7,8]. Regarding the active site, although the authors have attempted to show that an iron center implanted in the frameworks of the zeolite is a good model of monooxygenase, their results indicate that the catalysts with irons in aggregative state rather show a better reaction performance, and [Fe]ZEOL catalyst shows similar activity and selectivity with Fe_xO_y/SiO_2. Anderson and Tsai [9] have reported that a Cu^{2+}-exchanged Fe-ZSM-5 catalyst is active for the production of methanol (maximum yield, ca. 0.6%) from the oxidation of methane by nitrous oxide. However, methanol was not formed over copper free H–FeZSM-5. Copper played more significant role in the formation of methanol than iron. The information about the active site of this catalyst was not reported. Two other communications have showed that the doping of small amount of iron into ZnO [10] and silica [11] enhanced the formation of formaldehyde. The yield of formaldehyde, however, was < 1% in both cases. Our group has shown that relatively high yield of formaldehyde (ca. 4%) can be obtained from the oxidation of methane by oxygen using an Fe–Nb–B–O complex oxide or a Li- or Zn-doped $Fe_2(MoO_4)_3$ catalyst [12,13]. However, for all these catalysts except for the one reported by Anderson and Tsai, no formation of methanol was reported. The direct conversion of CH_4 into CH_3OH is extremely difficult over solid catalysts.

The fact that the presence of a reductant (usually NADH) is indispensable for the selective oxidation of methane to methanol for MMO catalytic systems has prompted us to co-feed a reductant and oxygen for the oxidation of methane over solid catalyst. Recently, we have reported that the conversion of methane is accelerated by co-feeding hydrogen with oxygen over several iron containing catalysts [14]. Particularly, the co-feeding of hydrogen induced the formation of methanol over $FePO_4$, $FeAsO_4$ and FAPO-5 (Fe:Al:P = 0.1:0.9:1.0) catalysts at atmospheric pressure and rather low temperatures (623–723 K). However, negative effect of H_2 on the conversion of CH_4 or no effect on the formation of methanol was observed for many other iron-containing catalysts. It is quite important to understand the environmental difference between the iron sites effective and ineffective in the selective oxidation of methane to methanol for designing better catalyst. Therefore, in this paper, three model catalysts in which iron sites exist in different structural environments are designed for the purpose of clarifying the active iron site. The catalytic performances of these model catalysts are correlated with the structural environments of iron sites characterized by various spectroscopic methods to understand the structure of the iron site needed for the selective oxidation of methane to methanol in the presence of H_2. These model catalysts are also examined for the oxidation of methane using H_2O_2 and N_2O which have been demonstrated to be effective oxidants for the direct oxidation of methane to methanol over $FePO_4$ catalyst [14,15]. The role of the counter anion of iron is discussed by comparing the results of $FePO_4$, $FeAsO_4$ and $FeSbO_4$.

2. Experimental

2.1. Catalyst

Al–P–O (Al:P = 0.9:1) was selected as the matrix for the preparation of the model catalysts with different structural environments of iron. Because the radius of Al^{3+} is similar to Fe^{3+}, $AlPO_4$ generally possesses similar crystalline structure to $FePO_4$. Thus, we can expect that the catalysts with different environments of iron will be obtained by introducing iron to the Al–P–O with different methods.

Three model catalysts A, B and C with a fixed composition (Fe:Al:P = 0.10:0.90:1.00) were prepared by the following methods. For preparing catalysts A and B, an Al–P–O sample (Al:P = 0.90:1.00) was preliminarily prepared from an aqueous solution of $Al(NO_3)_3$ and $NH_4H_2PO_4$. After the solution was evaporated to dryness, the resultant was calcined at 823 K to obtain the Al–P–O mixed oxide sample. Catalyst A was prepared by thoroughly mixing the Al–P–O sample with an Fe_2O_3 powder which was freshly prepared by the decomposition of $Fe(NO_3)_3$ at 823 K. The mixture was calcined at 823 K for 5 h in air. Catalyst B was prepared by an impregnation method as follows. The Al–P–O sample prepared above was immersed in an aqueous solution of $Fe(NO_3)_3$ for 12 h. The solution was dried up by heating at 343 K. The resultant was further dried at 393 K for 12 h and subsequently calcined at 823 K for 5 h. Catalyst C was directly prepared from the reaction of $Fe(NO_3)_3$, $Al(NO_3)_3$ and $NH_4H_2PO_4$ in the aqueous solution, followed by evaporating water at 343 K to dryness with stirring. The resultant was further dried at 393 K for 12 h and finally calcined at 823 K for 5 h. The BET surface areas of catalysts A, B and C were 4.8, 4.9 and 12.1 $m^2\ g^{-1}$, respectively.

Iron phosphate ($FePO_4$) and iron arsenate ($FeAsO_4$) compounds were prepared from the mixed aqueous solutions of $Fe(NO_3)_3$ and $NH_4H_2PO_4$ and of $Fe(NO_3)_3$ and H_3AsO_4, respectively. After evaporated at 343 K and further dried at 393 K for 12 h, the resultants were calcined at 823 K for 5 h in air. $FeSbO_4$ compound was prepared by a coprecipitation method from a mixed solution of $Fe(NO_3)_3$ and $SbCl_3$ using NH_2CONH_2 as a precipitant. After being thoroughly washed with water, the precipitate was dried at 393 K for 12 h, and calcined at 973 K for 10 h. The surface areas of $FePO_4$, $FeAsO_4$ and $FeSbO_4$ thus prepared were 8.5, 9.3 and 6.1 $m^2\ g^{-1}$, respectively.

The Na-ferrisilicate with MFI-type structure was synthesized by a hydrothermal method as described elsewhere [16]. The final calcination was carried out at 773 K for 4 h in air. The Si/Fe atomic ratio was 75. H-ferrisilicate was obtained by exchanging the Na^+ in Na-ferrisilicate with NH_4Cl aqueous solution (0.1 mol dm^{-3}) at 293 K for two days, followed by calcination at 773 K.

2.2. Catalytic reaction

The catalytic oxidation of CH_4 was carried out using a conventional fixed-bed flow reactor (quartz tube) operated at atmospheric pressure. The internal diameter of the reactor at the catalyst bed was 8 mm, decreasing to 3 mm at the outlet to remove the products quickly from the hot zone of the reactor. The reactants used in this study included CH_4 (purity > 99.99%), O_2 (> 99.5%), H_2 (> 99.9%), H_2O_2 aqueous solution (30 wt%) and N_2O (> 99.5%). These were used without further purification. Before each run of reaction, the catalyst was pretreated in the reactor with a flow of oxygen (8.4 kPa) at 723 K for 1 h, followed by purging with a flow of pure helium. Special caution was taken to prevent explosion when H_2 was co-fed with O_2. In the reaction using H_2O_2, the H_2O_2 aqueous solution (30 wt%) was fed into the reactor by a micro-feeder.

2.3. Catalyst characterization

BET surface area measurements were carried out with a volumetric apparatus (Belsorp type

36, Bel Japan) using nitrogen as an adsorbate at 77 K. The analyses of the elements in the catalysts were performed by means of the induced-coupled-plasma (ICP) emission spectrophotometer. Before the measurements, the catalysts were completely dissolved using a 7% HNO_3 aqueous solution.

XRD patterns were determined with a X-ray diffractometer (Rigaku Geigerflex 2031) using Ni filtered CuKα radiation. Mössbauer spectra were recorded at room temperature using a ^{57}Co source and an acceleration spectrometer operated in triangular mode. The data processing was performed using a Normos Mössbauer Fitting Program (WISSEL). XPS measurements were performed with an ESCA LAB 220-I spectrometer (FISONS Instruments), using MgKα radiation. Peak positions were calibrated using a C 1s photoelectron peak at 286.4 eV as the reference. The quantification of the surface ratio of Fe:Al:P is determined from the peak areas of Fe 3p, Al 2p and P 2p and the sensitive factors presented by FISONS Instruments.

The acidities of the catalysts were evaluated by ammonia-TPD measurements. The adsorption of NH_3 on the sample (100 mg) pre-evacuated at 723 K was carried out at 423 K for 1 h at an equilibrium pressure of 13.3 kPa. Followed by a brief evacuation at 423 K, the TPD of NH_3 was carried out by increasing the temperature at a rate of 10 K min^{-1} and was monitored by a quadrupole mass spectrometer.

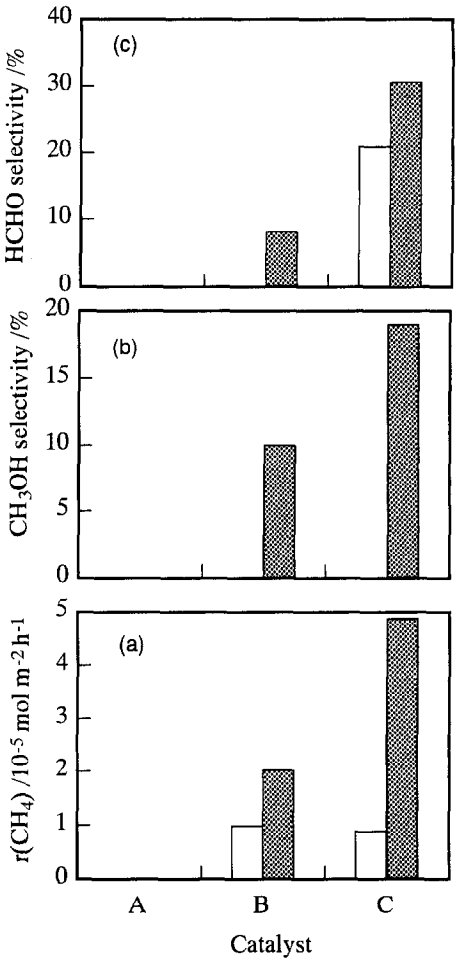

Fig. 1. Oxidation of CH_4 by O_2 in the presence and absence of H_2 over the model catalysts. □ In the absence of H_2; ▩ in the presence of 50 kPa H_2. (a) CH_4 conversion rate; (b) CH_3OH selectivity; (c) HCHO selectivity. Reaction conditions: $P(CH_4) = 33.8$ kPa, $P(O_2) = 8.4$ kPa, $T = 723$ K.

3. Results

3.1. Catalytic activity of the model Fe–Al–P–O catalysts

3.1.1. Oxidation of CH_4 by O_2 in the absence and presence of H_2

The catalytic activities of the three model Fe–Al–P–O catalysts (catalysts A, B and C) for the oxidation of CH_4 by O_2 have been measured in the presence and absence of H_2. The results obtained at 698 K are shown in Fig. 1. The oxidation activity of CH_4 with O_2 and that with H_2–O_2 over the Al–P–O sample had been measured as background ones of the Al–P–O components in the catalysts A, B and C. Neither oxidation occurred on the Al–P–O catalyst under the conditions of Fig. 1. These results confirm that iron is an indispensable active component for the oxidation of CH_4. Catalyst A, prepared by the physically mixing method, was completely inactive for the oxidation of CH_4 irrespective of the presence or absence of H_2. Although a large part of oxygen (25%) was used for water formation, the presence of H_2

did not initiate the oxidation of CH_4. This indicates that the iron sites in catalyst A do not function as active sites for the oxidation of methane to methanol in the co-existence of H_2 and O_2.

On the other hand, catalysts B and C were active for the oxidation of CH_4. As shown in Fig. 1a, the co-feeding of H_2 with O_2 appreciably increased the rate of CH_4 conversion for both catalysts. CH_4 conversion rate was increased about twice for catalyst B and five times for catalyst C due to the co-feeding of H_2 of 50 kPa. Another characteristic feature of the co-feeding of H_2 was that CH_3OH was newly produced (Fig. 1b). The comparison between catalysts B and C shows that the accelerating effect of H_2 on the selective oxidation of CH_4 to CH_3OH is more notable over catalyst C.

The presence of H_2 increased the conversion of O_2 over all the three catalysts. In the oxidation of CH_4 with H_2 and O_2 mixture, the conversion of O_2 could be divided into two parts, i.e., the O_2 used in the oxidation of CH_4 to CH_3OH, HCHO, CO and CO_2, and that used in the oxidation of H_2 to water. These O_2 conversions can be calculated on the bases of the amount of products. The conversions of oxygen due to CH_4 and H_2 oxidation thus calculated are shown in Fig. 2. The efficiency which is calculated by the following equation is also shown in Fig. 2.

$$\text{Efficiency} = \frac{\text{O}_2 \text{ conversion ascribed to } CH_4 \text{ oxidation}}{\text{total O}_2 \text{ conversion}} \times 100\%$$

Among the three catalysts, the consumption of O_2 due to the oxidation of H_2 is the lowest for catalyst C. However, as described above, the acceleration of the oxidation of CH_4 to CH_3OH due to the presence of H_2 is most remarkable for this catalyst. This fact excludes the possibility that the increase of CH_4 conversion rate in the presence of H_2 is due to the generation of the hot spot by the reaction of H_2 and O_2. In

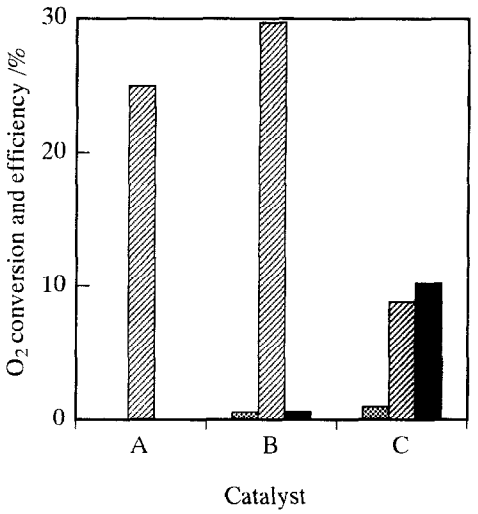

Fig. 2. The conversion of O_2 and the efficiency for the oxidation of CH_4 in the presence of H_2 over the model catalysts. ▩ O_2 conversion ascribed to CH_4 oxidation; striped bar – O_2 conversion ascribed to H_2 oxidation; ■ efficiency.

fact, as shown in Fig. 2, the conversion of O_2 is $< 10\%$ for catalyst C. The proportion of the O_2 used for CH_4 oxidation in the total conversion of O_2 is 10.2% for catalyst C. This value is much greater than that calculated for catalyst B (0.6%) or A (0%). These results indicate that H_2 is most effectively used on catalyst C for the selective oxidation of CH_4 to CH_3OH. On the other hand, more than 99.4% of the reacted H_2 was consumed in the formation of water for catalysts A and B.

In order to get insight into the reaction initiated in the presence of H_2, the effect of H_2 on the oxidation of CH_4 has been investigated in detail over catalyst C. The results suggest that the reaction features in the presence of H_2 over catalyst C are similar to those over $FePO_4$ catalyst reported previously [14]. The presence of H_2 greatly increased the conversion rate of CH_4 and notably lowered the temperature needed for the conversion of CH_4, e.g., the conversion of CH_4 to CH_3OH started at 600 K in the presence of H_2 under the conditions of Fig. 1, while no reaction occurred in O_2 alone until 683 K. The presence of H_2 induced the production of CH_3OH, while no CH_3OH was observed using

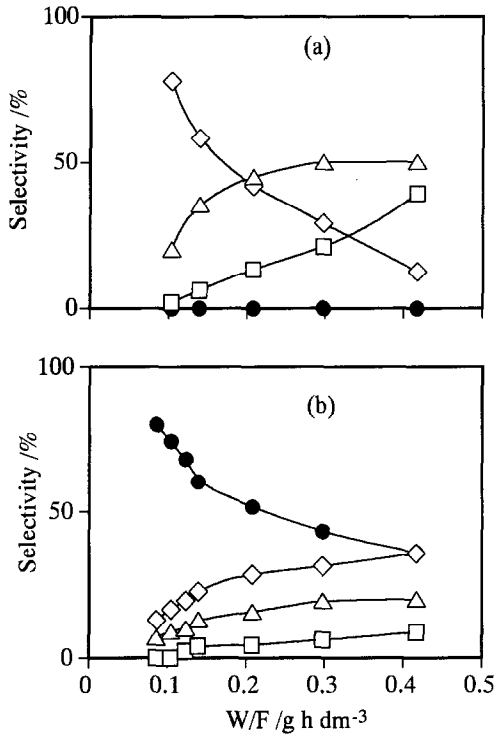

Fig. 3. Product selectivities as functions of the contact time over catalyst C. (a) In the absence of H_2, $T = 653$ K; (b) in the presence of 50 kPa H_2, $T = 748$ K. (●), CH_3OH; (◇), HCHO; (△), CO; (□), CO_2. Reaction conditions: $P(CH_4) = 33.8$ kPa, $P(O_2) = 8.4$ kPa.

O_2 alone under any reaction conditions at atmospheric pressure. In order to obtain the information about the formation scheme of CH_3OH, the reaction paths were investigated by changing the contact time (expressed as W/F) over catalyst C. The reaction was carried out in the presence of H_2 at 653 K, where no reaction occurred without H_2, and in the absence of H_2 at 748 K for obtaining a comparable CH_4 conversion rate. The product selectivities were shown in Fig. 3. As shown in Fig. 3a, in the absence of H_2, HCHO was formed as a primary product and no CH_3OH was produced at all the contact time. On the other hand, in the presence of H_2, the results in Fig. 3b clearly suggest that CH_3OH becomes the initial product and HCHO is formed as the secondary product through CH_3OH.

Furthermore, the reactions of HCHO and CO with H_2 or H_2–O_2 gas mixture did not give any CH_3OH under all the reaction conditions over catalyst C. Therefore, all these results strongly suggest that the co-feeding of H_2 and O_2 generates a new active oxygen species for the selective oxidation of CH_4 to CH_3OH at relatively lower temperatures over catalyst C.

3.1.2. *Oxidation of CH_4 using H_2O_2 and N_2O*

As described earlier, we have demonstrated that H_2O_2 and N_2O are effective oxidants for the conversion of CH_4 to CH_3OH at 573–773 K over $FePO_4$ catalyst [14,15]. In order to get information about the nature of the active site for the conversion of CH_4 to CH_3OH by these oxidants, we have examined the catalytic activities for the oxidation of CH_4 using H_2O_2 and N_2O over the three model catalysts.

The comparison of the activities of the three Fe–Al–P–O catalysts using H_2O_2 is shown in Fig. 4. CH_3OH was produced for catalysts B and C, while catalyst A was inactive for the oxidation of CH_4 using H_2O_2. Catalyst C was the most active one among the three catalysts. It should be noted that the real partial pressure of H_2O_2 must be lower than that shown in the figure because the decomposition of H_2O_2 occurred on the catalyst. Moreover, because a large amount of water was co-fed with H_2O_2, the results shown in Fig. 4 did not represent the real activities of oxidation of CH_4 by pure H_2O_2. In fact, notable inhibition effect of water has been observed in the case of using H_2–O_2 gas mixture [14].

Fig. 5 shows the results for the oxidation of CH_4 using N_2O. In this case, catalyst A showed a low activity for the oxidation of CH_4. The addition of H_2 increased the conversion rate of CH_4 and a detectable amount of CH_3OH was formed. Compared with catalyst A, catalysts B and C showed much higher activities for the oxidation of CH_4 to CH_3OH. CH_3OH was formed from CH_4 as a main product when N_2O was used without H_2. However, the presence of H_2 increased the conversion of CH_4 as well as

the selectivity of CH_3OH. Catalyst C was the most active and selective one for the conversion of CH_4 to CH_3OH among the three catalysts. A selectivity of 19% to CH_3OH (7% to HCHO) was obtained at a CH_4 conversion of 15% when N_2O and H_2 was co-fed over catalyst C at 698 K. It should be noted here that the reactivity of N_2O with H_2, producing H_2O and N_2, was not so high compared with that for the oxidation of CH_4. Under the reaction conditions of Fig. 5, 31% of the reacted N_2O was used in oxidation of CH_4 to CH_3OH over catalyst C in the presence of 16.9 kPa of H_2. In the presence of 34 kPa H_2 (the partial pressures of H_2 and CH_4 were the same), 22% of the reacted N_2O was used in the oxidation of CH_4 to CH_3OH. These observations suggest that the reactivities of CH_4 and H_2 toward the active oxygen species generated from N_2O are comparable.

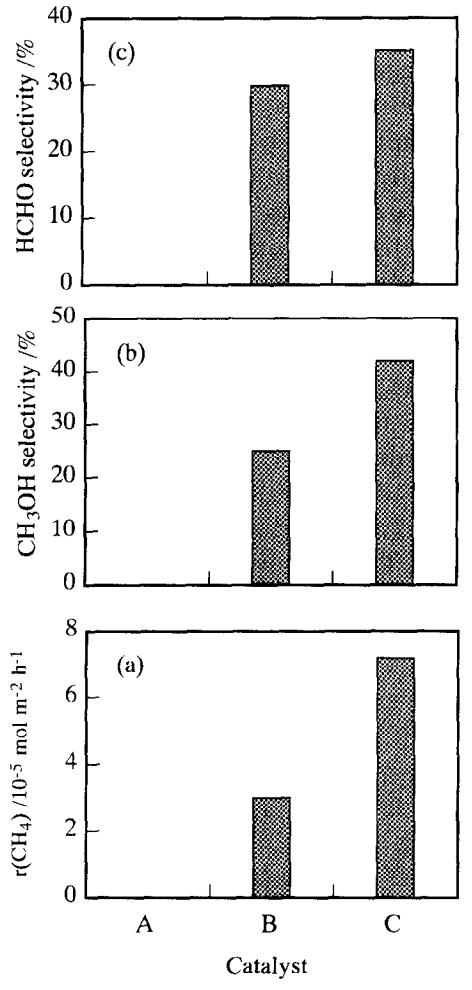

Fig. 4. Oxidation of CH_4 by H_2O_2 over the model catalysts. (a) CH_4 conversion rate; (b) CH_3OH selectivity; (c) HCHO selectivity. Reaction conditions: $P(CH_4) = 33.8$ kPa, $P(H_2O_2) = 8.4$ kPa, $P(H_2O) = 11.8$ kPa, $T = 723$ K.

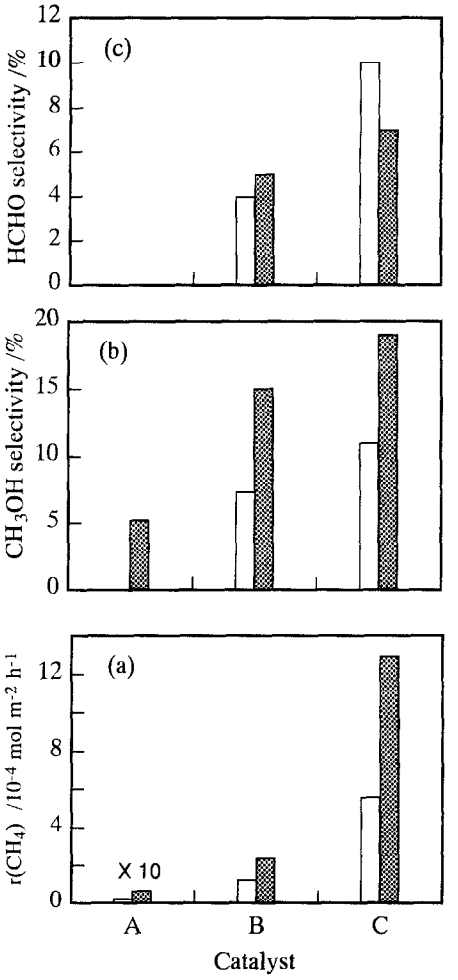

Fig. 5. Oxidation of CH_4 by N_2O over the model catalysts. □ In the absence of H_2; ▩ in the presence of 50 kPa H_2. (a) CH_4 conversion rate; (b) CH_3OH selectivity; (c) HCHO selectivity. Reaction conditions: $P(CH_4) = 33.8$ kPa, $P(N_2O) = 16.9$ kPa, $T = 698$ K.

If Figs. 1, 4 and 5 are compared, it is apparent that N_2O is the most potent oxidant for the oxidation of CH_4 to CH_3OH among the oxidants used. The reasons for this will be discussed later. However, the orders of the activities of the catalysts are the same (C > B > A)

irrespective of the kind of oxidant used. This fact suggests that the active site for the oxidation of CH_4 to CH_3OH is the same irrespective of the kind of oxidant.

3.2. Characterization of the Fe–Al–P–O catalysts

As described above, the three model catalysts showed remarkably different activities in the selective oxidation of CH_4 to CH_3OH by H_2–O_2. To understand the reasons for this and to elucidate the iron site needed for this selective oxidation reaction, the three model catalysts were characterized in detail as follows.

3.2.1. Average bulk and surface compositions

The average bulk and the surface compositions of the three model catalysts were measured by ICP and XPS methods. The results in Table 1 show that the atomic ratios of Fe:Al:P measured by ICP are independent of the preparation methods and close to those adjusted at the preparation for all the three catalysts (Fe:Al:P = 0.10:0.90:1.00). However, the atomic ratios of Fe:Al:P detected by XPS were quite different from those adjusted at the preparation and depended on the preparation method. Generally, XPS measurement reflects the information at the surface region with a depth of 0.5–2.5 nm. Thus, the results of XPS analyses suggest that the surface composition of each catalyst is strongly influenced by the preparation method. As shown in Table 1, the concentration of iron is the highest on the surface of catalyst B, whereas it is the lowest on the surface of catalyst C, i.e., the number of iron cations at the surface region was the lowest for catalyst C. As described earlier, the catalytic activity of catalyst C per surface area for the oxidation of CH_4 to CH_3OH was the highest among the three model catalysts (Figs. 1, 4 and 5). Therefore, the results obtained here confirm that the iron site of catalyst C is the most active one for the selective oxidation of CH_4 to CH_3OH using H_2–O_2, H_2O_2 or N_2O.

Table 1
Bulk and surface compositions analyzed by ICP and XPS

Catalyst	Fe:Al:P (atomic ratio)	
	by ICP	by XPS
A	0.090:0.88:1.00	0.033:0.86:1.00
B	0.092:0.89:1.00	0.147:0.71:1.00
C	0.095:0.90:1.00	0.025:0.87:1.00

3.2.2. X-ray diffraction

XRD patterns for catalysts A, B and C are shown in Fig. 6. The diffraction pattern of catalyst A shows that this catalyst comprises α-Fe_2O_3 and $AlPO_4$ phase of quartz structure. Because the ratio of phosphorus to aluminum in this catalyst calculated from ICP measurement is greater than one (1.14), it can be expected that an amorphous phosphorus oxide also exists. The relatively low concentration of the iron on the surface of this sample indicated by XPS data in Table 1 may suggest the existence of an overlay of amorphous P_2O_5 on iron oxide particles.

On the other hand, the XRD pattern ascribed to α-Fe_2O_3 was not observed for both catalysts B and C, although the average compositions of the three catalysts were almost the same (Table 1). This observation suggests that iron is dispersed in catalysts B and C. However, as shown in Fig. 6, the XRD patterns for catalysts B and C are quite different from each other. The XRD pattern for catalyst B is the same as that for the matrix Al–P–O, showing only the $AlPO_4$ phase of quartz structure, while the XRD pattern for catalyst C is completely different. The pattern for catalyst C can be assigned to another $AlPO_4$ phase of tridymite structure (pseudohexagonal symmetry, ASTM 20-44). The tridymite structure of $AlPO_4$ is known to be formed at high temperature. Generally, a higher temperature than 1173 K is needed for the formation of this structure when aluminum phosphate alone is calcined [17]. However, the calcination temperature for catalyst C in this study (823 K) was remarkably lower than this required tempera-

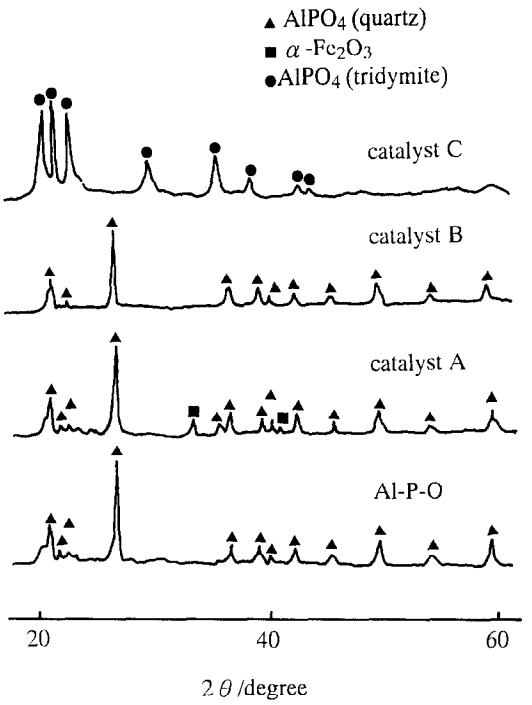

Fig. 6. X-ray diffraction patterns for the Al–P–O sample and the model catalysts A, B and C.

ture. Thus, the iron must play an important role in the formation of this structure. The d values calculated from Fig. 6 for the three most strong peaks of catalyst C are 4.383, 4.152 and 3.895 Å, while those for pure $AlPO_4$ of tridymite structure are 4.368, 4.130 and 3.860 Å, respectively. The d values for catalyst C are obviously larger than those for the pure $AlPO_4$ of tridymite structure. Such phenomenon was also reported by Gadgil and Kulshreshtha [17]. These facts indicate that a part of Al^{3+} cations have been replaced by Fe^{3+} cations during the formation of tridymite structure of $AlPO_4$. The increase in lattice spacings can be ascribed to the larger ionic radius of Fe^{3+} than Al^{3+} ($r(Fe^{3+}) = 0.64$ Å and $r(Al^{3+}) = 0.54$ Å). In other words, the iron cations in catalyst C must be highly dispersed in the tridymite structure of $AlPO_4$.

The structural environment of iron in catalyst B is different from those of catalysts A and C because of the followings. The facts that α-Fe_2O_3 has not been observed and the Al–P–O structure has not been changed in the presence of iron suggest that iron is mainly dispersed at the surface region of the quartz structure of $AlPO_4$. This speculation is supported by the result from XPS measurement that the content of iron at the surface region was unusually high for this catalyst compared to those of catalysts A and C (Table 1).

3.2.3. Mössbauer spectroscopic study

Mössbauer spectroscopy was utilized to get further insight into the state and the coordination environment of iron in the three model catalysts. The results are summarized in Table 2. For comparison, the results of α-Fe_2O_3 and $FePO_4$ were also shown in the table.

The spectrum of catalyst A has shown that there exist two types of irons in this catalyst. The sextet with an isomeric shift $\delta = 0.37$ mm/s and an internal hyperfine field $H = 518$ kOe can obviously be ascribed to α-Fe_2O_3. The proportion of such iron was 95% as shown in Table 2. It is known that the iron in α-Fe_2O_3 is in octahedral coordination of oxygen anions and the FeO_6 units connect with each other by sharing oxygen anions. In addition to α-Fe_2O_3, a very small amount of iron (5%) in a different state was also observed. This iron showed a quadrupole doublet with isomeric shift $\delta = 0.42$ mm/s and quadrupole splitting $\Delta = 0.95$ mm/s. It is reasonable that the presence of such a small amount of iron phase could not be detected by XRD studies. We speculate that such iron may exist at the interface between α-Fe_2O_3 and $AlPO_4$ or P_2O_5.

Table 2
Results of Mössbauer spectra for the model catalysts

Catalyst	Peak	δ (mm/s)	Δ (mm/s)	H (kOe)	Relativity (%)
A	sextet	0.37	−0.19	518	95
	doublet	0.42	0.95		5
B	doublet	0.33	0.99		100
C	doublet	0.33	0.64		100
Fe_2O_3	sextet	0.37	−0.18	520	100
$FePO_4$	doublet	0.33	0.64		100

On the other hand, as shown in Table 2, only one doublet has been observed for both catalysts B and C. The isomeric shifts shown in the table are also close to each other. The value of such an isomeric shift (0.33 mm/s) is known to be characteristic of Fe^{3+} in the tetrahedral coordination of oxygen anions in phosphates [17,18]. However, as shown in Table 2, the values of quadrupole splitting (Δ) for catalysts B and C are obviously different from each other. The lower quadrupole splitting for catalyst C indicates a higher symmetry of the coordination circumstance of iron in this catalyst. Moreover, as shown in Table 2, the quadrupole splitting for catalyst C is the same as that for $FePO_4$. Therefore, we suggest that the coordination environment of iron in catalyst C resembles that in $FePO_4$. It is known that an iron in $FePO_4$ structure is isolated by four tetrahedral units of PO_4. Thus, an iron in catalyst C must similarly be surrounded by the four tetrahedral units of PO_4. In contrast, the higher quadrupole splitting obtained for catalyst B (Table 2) suggests a lower symmetry for the environment of iron site in this catalyst. Considering the fact that iron is accumulated at the surface region of catalyst B, the FeO_4 units may not be isolated from each other. In other word, the tetrahedral FeO_4 units in catalyst B may connect with the units including FeO_4, AlO_4 and PO_4.

3.2.4. Structures of iron sites in the model catalysts

In conclusion, the immediate environments of the iron sites for the three model catalysts are demonstrated in Fig. 7. The iron in catalyst A is mainly in the structure of α-Fe_2O_3, viz., each iron is octahedrally coordinated with oxygen and the FeO_6 octahedron is connected with each other. On the other hand, the iron cations in catalysts B and C are tetrahedrally coordinated with oxygen. Such tetrahedrally coordinated iron sites in catalyst C are isolated from each other and surrounded by the PO_4 tetrahedra, while those in catalyst B may connect with other FeO_4, AlO_4 and PO_4 units. It should be noted

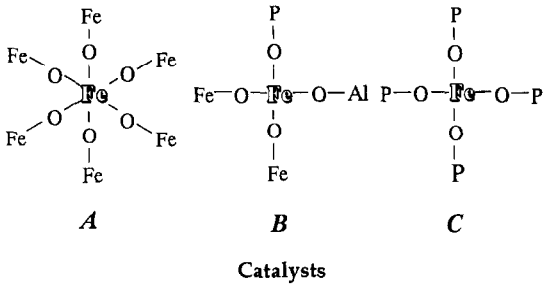

Fig. 7. The structures of the iron sites in the model catalysts.

that the structure for catalyst B in Fig. 7 is only an example. Other arrangements with tetrahedra of Fe, Al and P by different ratio around an iron site are also possible. Moreover, the structures described in Fig. 7 do not represent the whole image of the catalyst but only describe the immediate environment around the iron center.

3.3. Correlation between the catalytic performances and the structures of iron sites

The correlation between the activities and the structures of the iron sites for the three model catalysts suggests that the tetrahedrally coordinated iron site which is isolated from each other and surrounded by phosphate groups is the active site for the selective oxidation of CH_4 to CH_3OH by H_2–O_2 gas mixture. The same iron site is also needed for the selective oxidation of CH_4 to CH_3OH by H_2O_2 or N_2O.

The iron site in catalyst A is mainly in the form of α-Fe_2O_3. Thus, this catalyst is almost inactive. As suggested from the results of Mössbauer spectroscopy, a small part of irons is in a different iron state which may exist at the interface between α-Fe_2O_3 and $AlPO_4$ or P_2O_5. These specific iron sites might be responsible for the low activity in the conversion of CH_4 to CH_3OH using N_2O in the presence of H_2. On the other hand, the irons in catalysts B and C were dispersed in the Al–P–O matrix. This dispersion must enhance the isolation of iron sites from each other. Especially, in the case of catalyst C, as described above, all the irons were dispersed in Al–P–O lattice (tridymite

structure) and occupied the position of Al^{3+} in the tridymite structure of $AlPO_4$. Such irons were proven to be surrounded by phosphate groups from the Mössbauer spectroscopic measurements. The iron site of this catalyst showed the highest activity.

3.4. Catalysts with iron site isolated by different anion groups

The iron site surrounded by phosphate groups has been suggested to be the active site for the selective oxidation of CH_4 to CH_3OH by H_2–O_2 and by H_2O_2 or N_2O. However, whether the surrounding environment of an active iron site is limited only to phosphate or other anion groups are also effective is still open for discussion. In order to make this point clear, iron compounds with other anions were studied. $FeAsO_4$ and $FeSbO_4$ are expected to have similar property to $FePO_4$ because P, As and Sb are in the same group in the periodic table. We have studied coordination environments of iron cations in these iron salts by Mössbauer spectroscopy. Similar to the results for $FePO_4$, one doublet with isomeric shift $\delta = 0.31$ mm/s and the quadrupole splitting $\Delta = 0.60$ mm/s was observed for $FeAsO_4$. However, for $FeSbO_4$, the isomeric shift and quadrupole splitting were 0.45 and 0.75 mm/s, respectively. The value of the isomeric shift of this compound was a typical one ascribed to the Fe^{3+} with the octahedral coordination of oxygen. These results suggest that the coordination environment of iron in $FeAsO_4$ is similar to that in $FePO_4$, whereas that in $FeSbO_4$ is quite different.

These two samples as well as $FePO_4$ were tested as catalysts for the oxidation of CH_4. The comparisons of the catalytic activities for the oxidation of CH_4 by O_2 in the presence and absence of H_2 over $FePO_4$, $FeAsO_4$ and $FeSbO_4$ were shown in Fig. 8. As reported previously [14], the co-feeding of H_2 with O_2 increased the conversion rate of CH_4 and initiated the production of CH_3OH over $FePO_4$. Such accelerating effect was also observed over $FeAsO_4$, although

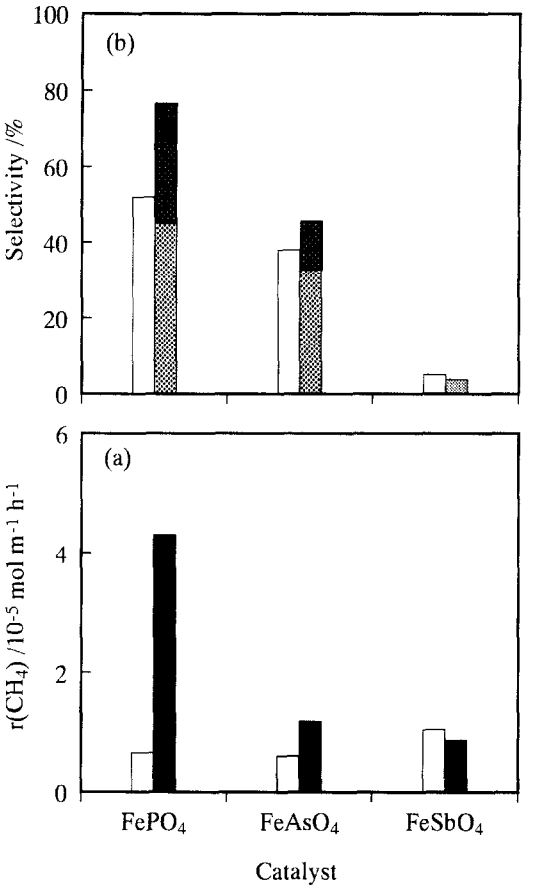

Fig. 8. Oxidation of CH_4 by O_2 in the presence and absence of H_2. (a) CH_4 conversion rate, in the absence of H_2, (□); in the presence of H_2, (■). (b) Selectivities, in the absence of H_2, (white bar), HCHO; in the presence of H_2, (dark grey), CH_3OH; (light grey), HCHO. Reaction conditions: $P(CH_4) = 33.8$ kPa, $P(O_2) = 8.4$ kPa, $P(O_2) = 8.4$ kPa, $P(H_2) = 50.7$ kPa, $T = 698$ K, $W = 0.5$ g, $F = 3.6$ dm^3 h^{-1}.

the effect of H_2 was not so notable as compared with $FePO_4$. However, as shown in Fig. 8, no CH_3OH was produced in the presence of H_2 over $FeSbO_4$ and H_2 showed a negative effect on the conversion rate of CH_4. As indicated by Mössbauer spectra, the iron in $FeSbO_4$ is in octahedral coordination of oxygen. The octahedron of iron cannot be isolated in this compound, while the iron cations in $FePO_4$ and $FeAsO_4$ are in tetrahedral coordination and each tetrahedral unit of FeO_4 is isolated by PO_4 or AsO_4 units. Thus, the results obtained here further support the conclusion that the isolated and

tetrahedrally coordinated iron site is necessary for the selective oxidation of CH_4 to CH_3OH by H_2–O_2.

However, although the iron sites in $FePO_4$ and $FeAsO_4$ possess similar structural environment, the enhancing effect of H_2 for both catalysts is notably different. As shown in Fig. 8, the co-feeding of H_2 with O_2 enhances both CH_4 conversion and CH_3OH selectivity markedly for $FePO_4$ compared to the effect on $FeAsO_4$. Therefore, other factors must influence the reaction in the presence of H_2. One reasonable factor for this may be the difference in the acidities of the surrounding groups of iron, i.e., PO_4 and AsO_4 groups. Thus, the acidities of these catalysts were investigated by NH_3-TPD method. As shown in Fig. 9, one broad desorption peak of ammonia was observed for all the three catalysts. The peak temperatures were 523, 465 and 452 K for the desorption of ammonia chemisorbed on $FePO_4$, $FeAsO_4$ and $FeSbO_4$, respectively. Moreover, the amount of the total ammonia desorbed from the samples per surface area was in the order of $FePO_4 \gg FeAsO_4 > FeSbO_4$. These observations show that the acidity of $FePO_4$ is stronger as compared with $FeSbO_4$. Such results strongly suggest that the acidic property of the environment groups surrounding the iron site is another important factor in the oxidation of CH_4 to CH_3OH by H_2–O_2 gas mixture.

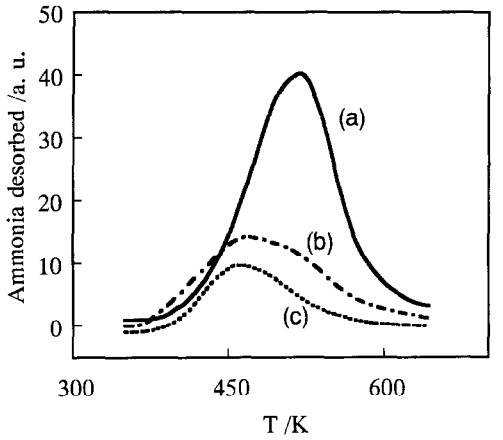

Fig. 9. NH_3-TPD curves. (a) $FePO_4$; (b) $FeAsO_4$; (c) $FeSbO_4$.

It is known that all metal cations occupy tetrahedral coordination sites surrounded and isolated by SiO_4-tetrahedra in zeolite structure or PO_4-tetrahedra in aluminophosphate-based molecular sieves. Therefore, the iron sites in these catalysts fit the active site model (model C) needed for the oxidation of CH_4 to CH_3OH by H_2–O_2 as suggested in Fig. 7. In fact, as reported earlier [14], FAPO-5, an Fe-substituted $AlPO_4$-5 in which the tetrahedrally coordinated iron is isolated by PO_4 tetrahedra, showed a remarkably accelerating effect of H_2 on the oxidation of CH_4 and a small amount of CH_3OH was obtained in the presence of H_2. Furthermore, we have examined the catalytic performance of a ferrisilicate with MFI-structure in which iron sites are isolated by SiO_4 tetrahedra. The results for the oxidation of CH_4 by O_2 in the absence and presence of H_2 over both Na- and H-ferrisilicates are shown in Table 3. Obviously, CH_4 conversion increased more notably

Table 3
Catalytic oxidation of CH_4 by O_2 co-fed with H_2 over ferrisilicate catalysts

Catalyst	$P(H_2)$ (kPa)	CH_4 conversion (%)	Selectivity (%)			
			CH_3OH	HCHO	CO	CO_2
Na-ferrisilicate	0	0.10	0	0	35.0	65.0
	8.4	0.14	0	0	36.7	63.3
	16.8	0.18	0	0	37.4	62.6
H-ferrisilicate	0	0.25	0	0	45.0	55.0
	4.2	0.88	0	8.9	78.9	15.3
	8.4	1.33	0	8.8	77.6	16.6
	16.8	2.38	0	9.7	78.2	15.1

Reaction conditions: $T = 673$ K, $P(CH_4) = 33.8$ kPa, $P(O_2) = 8.4$ kPa, $W = 0.2$ g, $F = 3.6$ dm^3 h^{-1}.

due to the co-feeding of H_2 for H-ferrisilicate as compared with that for Na-ferrisilicate. Moreover, the product selectivities were influenced more greatly due to the co-feeding of H_2 over H-ferrisilicate. For this catalyst, in the absence of H_2, CO_2 was the main product and no HCHO was observed, while HCHO was newly produced and CO became the main product in the presence of H_2. It should be noted that CO was not formed from the reaction between CO_2 and H_2 because no CO was observed when the reaction of CO_2 with H_2–O_2 was carried out on this catalyst. Thus, it is likely that CO is produced from the further oxidation or decomposition of HCHO. These results apparently suggest that the acidity of the environment of iron is an important factor. However, no CH_3OH was obtained over H-ferrisilicate in the presence of H_2. It is probable that the CH_3OH formed in the channels of this zeolite is further converted into HCHO and CO before its desorption through the channels into the gas phase. Similarly, CH_3OH production was not observed over a Fe-ZSM-5 catalyst for the oxidation of CH_4 by H_2–O_2, although the accelerating effect of H_2 on the conversion of CH_4 was notable [14].

4. Discussion

The results described above have suggested that the tetrahedrally coordinated iron site isolated by acidic groups is the active site for the selective oxidation of CH_4 to CH_3OH by H_2–O_2. Here, we discuss about the functions of this active site in the selective oxidation of CH_4 to CH_3OH by H_2–O_2 to get further information about the reaction mechanism.

As described earlier, the facts that the conversion of CH_4 occurs at lower temperatures and CH_3OH is selectively produced in the presence of H_2 have strongly suggested that a new active oxygen species is generated for the selective oxidation of CH_4 to CH_3OH in the presence of H_2 and O_2. In order to elucidate this active oxygen species, we have carried out in situ FT-IR studies over an Fe–Al–P–O catalyst in which the iron sites are in the same structural environments with the model catalyst C. The results of the FT-IR experiments indicated that an adsorbed peroxide species was responsible for the reaction with CH_4 to form methoxide and acidic OH groups as the intermediates for the formation of CH_3OH on the catalyst surface [19].

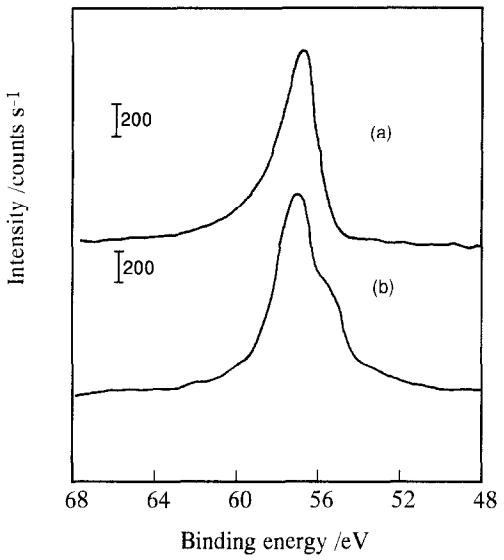

Fig. 10. Fe 3p spectra obtained from XPS measurements for catalyst C. (a) Fresh catalyst; (b) after a reaction for 5 h in a $(CH_4 + H_2 + O_2)$ gas mixture.

In order to understand the role of iron site during the reaction, the catalyst C after a reaction for 5 h in CH_4–H_2–O_2 ($P(CH_4) = 33.8$, $P(O_2) = 8.4$, $P(H_2) = 50.7$ kPa) gas flow was analyzed by XRD, Mössbauer and XPS studies. Obvious changes were not observed before and after the reaction for XRD and Mössbauer measurements. However, notable difference was observed for XPS spectra of the catalyst before and after the reaction. As shown in Fig. 10, a new shoulder peak at 56.2 eV, which can be assigned to an Fe(II) on the catalyst surface, was observed in Fe 3p spectrum after the reaction, while only a single peak at 57.7 eV ascribed to an Fe(III) was observed before the reaction. These results indicate that the redox

between Fe(III) and Fe(II) occurs on the catalyst surface during the reaction. The important role of the Fe(II) generated during the reaction was suggested by the pulse reaction experiments below. Fig. 11 shows the effect of the pre-reduction of the catalyst by H_2 pulses on the reaction of a $(CH_4 + O_2 + H_2)$ pulse over catalyst C. The degree of reduction of the catalyst surface by the H_2 pulses was calculated from the amount of the water produced and the number of oxygen anions of the catalyst surface. Obviously, the pre-reduction enhanced the selective oxidation of CH_4 to CH_3OH as shown in Fig. 11. Therefore, we believe that the Fe(II) on the catalyst surface plays an important role in the formation of the peroxide in the presence of H_2 and O_2.

Because neither the oxidation of CH_4 nor the reaction between H_2 and O_2 occurred over iron free Al–P–O, it is reasonable to assume that the iron site in the iron-containing catalysts is the active site for these reactions. The reaction mechanism of CH_4 to CH_3OH in the presence of H_2 and O_2 which we have in mind is demonstrated in Fig. 12. H_2 reduces the surface, generating Fe(II) and H^+ which is adsorbed on the neighboring phosphate groups (step 1). The

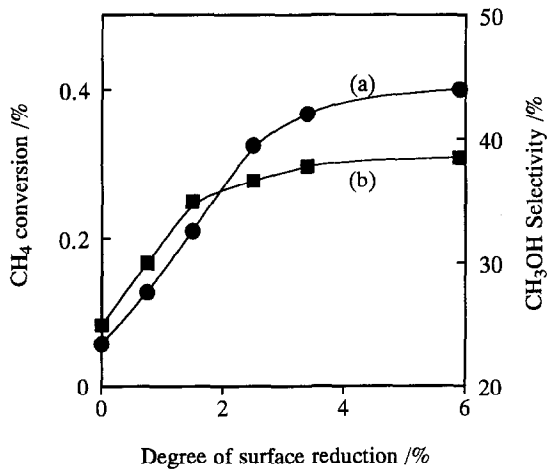

Fig. 11. Effect of the pre-reduction by H_2 pulse on the reaction of $(CH_4 + H_2 + O_2)$ pulse over catalyst C. (a) CH_4 conversion; (b) CH_3OH selectivity. $T = 698$ K, $W = 0.5$ g, He carrier 40 cm^3 min^{-1}, pulse size 2.7 cm^3, in the pulse: $P(CH_4) = 33.8$ kPa, $P(H_2) = 50.7$ kPa, $P(O_2) = 8.4$ kPa.

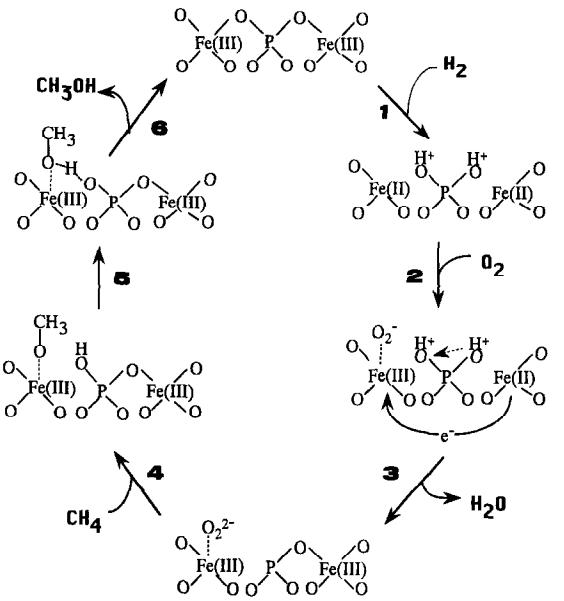

Fig. 12. The proposed reaction mechanism for the selective oxidation of CH_4 to CH_3OH by H_2–O_2 over active iron site.

Fe(II) activates O_2 into O_2^- species by one electron transfer (step 2). The peroxide species formed through the O_2^- species by accepting one electron from the other Fe(II) site (step 3) would activate CH_4 into CH_3OH (steps 4–6).

The peroxide species generated on the isolated iron site may be protected from the attack of the hydrogen adsorbed on the neighboring iron sites. Thus, the H_2–O_2 reaction to H_2O over catalyst C must be greatly prevented compared to the catalysts A and B. Therefore, the lifetime of the peroxide on the isolated iron site surrounded by phosphate groups must be prolonged, and thus, the peroxide species has more chance to react with CH_4. On the other hand, for the iron site not isolated by phosphate groups, e.g., models A and B in Fig. 7, even if the peroxide species may be generated as an intermediate in the activation of O_2, it will be rapidly reduced to H_2O before reacting with CH_4. These speculations are supported by the experimental facts shown in Fig. 2. As shown in Fig. 2, the reaction between H_2 and O_2 to produce H_2O proceeded much faster over catalysts A and B, while this reaction was the

slowest over catalyst C. The accelerating effect of H_2 on the selective oxidation of CH_4 was most notable on catalyst C, because the isolated structure of iron for this catalyst prevents the H_2–O_2 reaction to H_2O and, consequently, increases the steady-state concentration of the peroxide species.

The acidity of the surrounding groups must facilitate the acceptance and donation of the H^+ during the activation of H_2 and O_2, and thus, enhance the formation of the peroxide. Therefore, a stronger acidity of the surrounding groups is advantageous to the selective oxidation of CH_4 to CH_3OH by H_2–O_2. Moreover, as shown in step 5 of Fig. 12, the acidic protons formed on the acidic groups such as phosphates neighbor to the iron site may facilitate the protonation of the methoxide intermediate to CH_3OH. The structure of the active iron site, i.e., the iron site isolated by acidic groups must ensure the formation of CH_3OH as the primary product by the protonation of the methoxide intermediate. Otherwise, without such structural environment of iron, even if methoxide can be formed as an intermediate, the rapid protonation will not be ensured and the further oxidation of methoxide to HCHO will overcome the formation of CH_3OH.

As describe earlier, H_2O_2 and N_2O are also effective oxidants for the selective oxidation of CH_4 to CH_3OH. It is reasonable that the adsorbed peroxide can be directly formed from H_2O_2, thus, H_2O_2 can be an effective oxidant for the selective production of CH_3OH on the same active iron site. In the case of N_2O, the formation of the peroxide species was also detected by FT-IR spectroscopy [19]. Moreover, similar to the one generated in H_2–O_2 gas mixture, the peroxide species from N_2O also reacted with CH_4 to form methoxide and OH as the intermediates of CH_3OH. Therefore, we consider that in the case of N_2O as the oxidant, the peroxide species is also responsible for the selective oxidation of CH_4 to CH_3OH.

It should be recalled that N_2O showed higher activity for the oxidation of CH_4 over the same catalyst as compared with H_2–O_2 and H_2O_2. Probably, the rate of conversion of the peroxide to H_2O in an atmosphere of N_2O is not so fast as in the case of H_2–O_2 or H_2O_2, thus the steady-state concentration of the peroxide from N_2O must be increased compared to that from H_2–O_2. Moreover, a large amount of H_2O formed in H_2–O_2 or co-fed with H_2O_2 (30 wt% H_2O_2 aqueous solution was used in the experiments) decreases the activity in these two cases. In fact, the addition of H_2O showed remarkably negative effect on the conversion of CH_4 [14,15]. However, at this moment, we should not exclude the possibility that a monoatomic oxygen species such as Fe(III) $\cdots$ O^- or Fe(IV)=O could be responsible for the selective oxidation of CH_4 to CH_3OH when N_2O is used as the oxidant. Further study on this point is needed.

References

[1] J. Colby, D.I. Stirling and H. Dalton, Biochem. J. 165 (1977) 395.

[2] M.J. Rataj, J.E. Kauth and M.I. Donnelly, J. Biol. Chem. 261 (1991) 18684.

[3] M.J. Brown and N.D. Parkyns, Catal. Today 8 (1991) 305; N.D. Parkyns, C.I. Warburton and J.D. Wilson, Catal. Today 18 (1993) 385.

[4] O.V. Krylov, Catal. Today 18 (1993) 209.

[5] T.J. Hall, J.S.J. Hargreaves, G.J. Hutchings, R.W. Joyner and S.H. Taylor, Fuel Proc. Tech. 42 (1995) 151.

[6] V.A. Durante, D.W. Walker, W.H. Seitzer and J.E. Lyons, 1989 Int. Chem. Congress on Pacific Basin Soc., preprints of 3B symp., p. 23; J.E. Lyons, P.E. Ellis and V.A. Durante, in: R.K. Grasselli and A.W. Sleight (Eds.), Structure-Activity and Selectivity Relationship in Heterogeneous Catalysis (Elsevier, Amsterdam, 1991) p. 99.

[7] S. Betteridge, C.R.A. Catlow, D.H. Gay, R.W. Grimes, J.S.J. Hargreaves, G.J. Hutchings, R.W. Joyner, Q.A. Pankhurst and S.H. Taylor, Top. Catal. 1 (1994) 103.

[8] G.S. Walker, J.A. Lapszewicz and G.A. Foulds, Catal. Today 21 (1994) 519.

[9] J.R. Anderson and P. Tsai, J. Chem. Soc. Chem. Commun. (1987) 1435.

[10] Z. Sojka, R.G. Herman and K. Klier, J. Chem. Soc. Chem. Commun. (1987) 1435.

[11] T. Kobayashi, K. Nakagawa, T. Tabata and M. Haruta, J. Chem. Soc. Chem. Commun. (1994) 1609.

[12] K. Otsuka, T. Komatsu, K. Jinno, Y. Uragami and A. Morikawa, in: Proc. 9th Int. Congression Catalysis, 1988, Vol. 2 (The Chemical Institute of Canada, Ottawa) p. 915.

[13] K. Otsuka, Y. Wang, I. Yamanaka, A. Morikawa and M.Yu. Sinev, Stud. Surf. Sci. Catal. 81 (1994) 503.
[14] Y. Wang and K. Otsuka, J. Chem. Soc. Chem. Commun. (1994) 1893; Y. Wang and K. Otsuka, J. Catal. 155 (1995) 256.
[15] Y. Wang and K. Otsuka, Chem. Lett. (1994) 1893; Y. Wang and K. Otsuka, J. Chem. Soc. Faraday Trans. 91 (1995) 3953.
[16] M.A. Uddin, T. Komatsu and T. Yashima, J. Catal. 146 (1994) 468.
[17] M.M. Gadgil and S.K. Kulshreshtha, J. Solid State Chem. 113 (1994) 15.
[18] J.M. Millet, C. Virely, M. Forissier, P. Bussiere and J.C. Vedrine, Hyperfine Interactions 46 (1989) 619.
[19] Y. Wang, K. Otsuka and K. Ebitani, Catal. Lett. 35 (1995) 259.